Applied Energy 147 (2015) 224–234

Contents lists available at ScienceDirect

Applied Energy

journal homepage: www.elsevier.com/locate/apenergy

Adaptive Pontryagin's Minimum Principle supervisory controller design for the plug-in hybrid GM Chevrolet Volt

Simona Onori [a,1], Laura Tribioli [b,*,1]

[a] Automotive Engineering Department, Clemson University, Greenville, SC 29607, USA
[b] Industrial and Mechanical Eng. Dpt., Univ. of Rome Niccolò Cusano, 00166 RM, Italy

HIGHLIGHTS

- Energy-based simulator for energy management of a Chevy Volt.
- In-vehicle LG Chem battery model built with experimental data.
- Pontryagin's Minimum Principle for supervisory energy management.
- Design of a practical controller tuned against the optimal solution.
- Comparative analysis of ARMA and PMP controllers.

ARTICLE INFO

Article history:
Received 3 September 2014
Received in revised form 29 December 2014
Accepted 5 January 2015
Available online 13 March 2015

Keywords:
Energy management
PHEV
Charge Depleting–Charge Sustaining
Pontryagin's Minimum Principle
Adaptive

ABSTRACT

This paper presents an adaptive supervisory controller, based on Pontryagin's Minimum Principle (PMP), for on-line energy management optimization of a plug-in hybrid electric vehicle. Using minimum driving information, such as the total trip length and the average cycle speed, the proposed algorithm relies on adaptation of the control parameter from state of charge feedback. The proposed strategy is referred in the paper to as Adaptive-PMP (A-PMP). The new controller is applied to a detailed forward vehicle simulator of the plug-in hybrid Chevrolet Volt manufactured by General Motors, where an experimentally validated LG Chem battery model is used. The strategy we propose aims at achieving a blended trajectory of the state of charge to minimize the consumed fuel, resulting in an overall better performance than the actual Charge Depleting/Charge Sustaining (CD/CS) strategy currently used on-board of the vehicle. A comparative analysis of three strategies, *i.e.*, the optimal one (PMP), the proposed one (A-PMP) and the in-vehicle one (CD/CS), is conducted in simulation which shows that improvement above 20% in fuel consumption may be achieved when the proposed algorithm is used instead of the current on-board strategy.

1. Introduction

Rising fuel price, pollutant emissions and an increasing concern for global warming have initiated a development process within the automotive industry towards electrified powertrains. Energy efficient transportation involves the introduction and use of advanced vehicle powertrains, *i.e.* hybrid and electric vehicles or vehicles running on alternative fuel, which are regarded today as promising technologies to displace a significant amount of petroleum relative to conventional vehicles [1]. Previous research has shown that optimization of hybrid vehicles is crucial for reaching high overall vehicle efficiency. Energy management control [2–5] and component design optimization [6–8], are the two major areas of research in the context of hybrid vehicles.

In today's hybrid vehicles, heuristic rule-based control strategies are used for on-board energy management [5,9,10], which call for simple implementation, low memory requirements and high computational efficiency. However, the heuristic-based design does not transfer from vehicle to vehicle resulting in an architecture-dependent rule development process (requiring *ad-hoc* design) with a sometimes high calibration effort. Model-based control design, on the other hand, has been shown to improve fuel economy. Recent research has, in fact, turned toward the development of strategies that are based on optimal control principles and that can guarantee optimality of the power split under a different range of operating conditions as well as transportability of the

* Corresponding author.
E-mail addresses: sonori@clemson.edu (S. Onori), laura.tribioli@unicusano.it (L. Tribioli).
[1] Part of this work was conducted at the Center for Automotive Research, The Ohio State University.

http://dx.doi.org/10.1016/j.apenergy.2015.01.021
0306-2619/

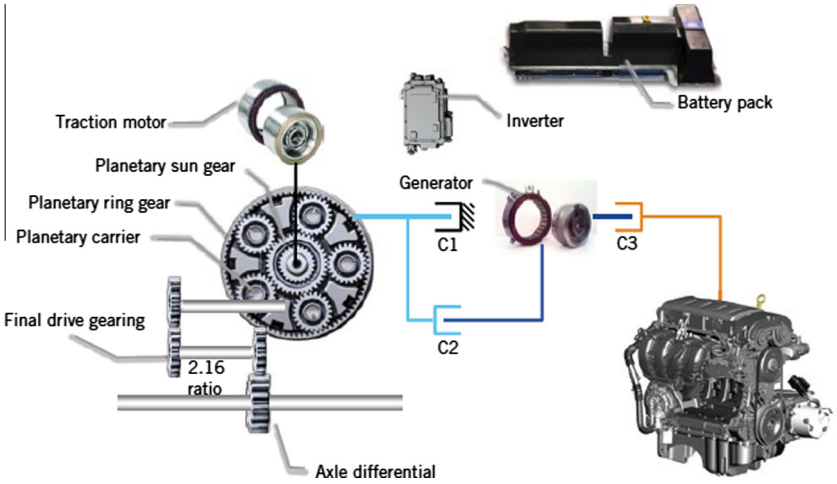

Fig. 1. Kinematic architecture of the Chevrolet Volt, Grebe and Nitz [21].

strategies to different vehicle architectures and component sizes leading to a lower calibration effort.

This paper focuses on the design of a novel model-based energy management strategy for reducing fuel consumption in a plug-in hybrid electric vehicle (PHEV) when minimum information on the traveled trip is available. PHEVs are hybrid electric vehicles (HEVs) where the electrochemical energy storage device, bigger than in the case of charge-sustaining HEVs, can be powered at home by plugging it on electricity.

The GM Chevrolet Volt (or Opel Ampera in Europe) is the first PHEV-40[2] in the market. The implemented discharge strategy consists of operating the vehicle as an electric vehicle until the battery is depleted and then proceeding in charge sustaining operation as a conventional HEV using the internal combustion engine. This strategy is referred to as the Charge Depleting/Charge Sustaining (CD/CS) strategy. However, if the length of the trip is greater than the nominal electric range, the overall energy cost (electricity and gasoline) can be reduced if the battery is discharged more gradually, such that it is depleted towards the end of the trip [11]; this type of strategy is often called a blended strategy as the use of electricity and gasoline is blended over the entire trip length. Milder usage of the battery (lower C-rates and Ah-throughput) results from the implementation of a blended strategy, with the consequence of a slower battery aging process [12]. On the other hand, though, a blended policy can only be used if the trip details, such as distance, velocity and altitude profiles are known *a priori*.

In [13], it is shown that when the road grade profile is approximately flat then it is possible to obtain close-to-optimal energy cost, given the trip length is known. However, a quasi-linear battery discharge profile is no longer optimal if the topography is hilly or mountainous. Not-flat road profiles are considered in [14], where a tuning of the energy management strategy, accounting for variations in potential energy throughout the trip, is proposed. A different approach is considered in [15], where a reference trajectory for the battery discharge trend is precalculated with dynamic programming (DP) (using *a priori* information available from the navigation system) and tracked during real time vehicle operation using an Adaptive-ECMS strategy [2,16,17]. A similar idea was also used in [18] for a charge-sustaining HEV, where the reference battery discharge profile is determined as a function of vehicle position with the aim of maximizing the recuperated energy, given the knowledge of the topographic profile of the future road segments and the corresponding average traveling speeds.

In this paper, we propose a novel model-based energy management strategy based on the Pontryagin's Minimum Principle (PMP) [19], to minimize the fuel consumed in a PHEV. The developed control strategy uses minimum information about the trip, *i.e.* only the average speed and the traveled distance, the most reliable parameters to be predicted in advance or, most commonly, to be retrieved from a GPS device when setting up the driving mission at the beginning of a trip. The proposed strategy, developed for the GM Chevrolet Volt vehicle, is based on the on-line minimization of the equivalent cost function where the adaptation of the control parameter, the *co-state*, is achieved by means of an improvement of the adaptation scheme proposed in [17]. It is shown in simulation that better performances are obtained, in terms of fuel economy, when the proposed strategy is used against the CD/CS strategy implemented today on the vehicle.

2. GM Chevrolet Volt Powertrain and vehicle modeling

The powertrain architecture of the Chevrolet Volt consists of the power-split, planetary-based system, shown in Fig. 1. Figure 1 also shows the main vehicle components and the mechanical coupling of the elements of the powertrain system. Three clutches ($C1, C2, C3$) allow connecting and disconnecting the internal combustion engine (ICE), the generator (GEN) and the main traction motor (MOT) [20,21]. Both electric machines (GEN and MOT) can work in both motoring and generating mode and for both of them the sign convention is that positive torque and positive electric power indicate motoring operation.

Vehicle component characteristics are reported in Table 1.

In this work, a detailed model of the Chevrolet Volt built upon real vehicle data, developed in Matlab®/Simulink® environment by researchers at the IFP Energies Nouvelles, Sciarretta et al. [22],

Table 1
Main characteristics of the vehicle.

Curb weight	1715 kg
Engine – SI 1.4 l maximum power	63 kW@4800 rpm
Electric motor maximum power	111 kW@4300 rpm
Generator maximum power	53 kW@4000 rpm
Battery maximum power	110 kW
Battery energy capacity	16 kWh

[2] PHEV-x indicates a PHEV with a x-mile electric range estimated on a standardized driving cycle.

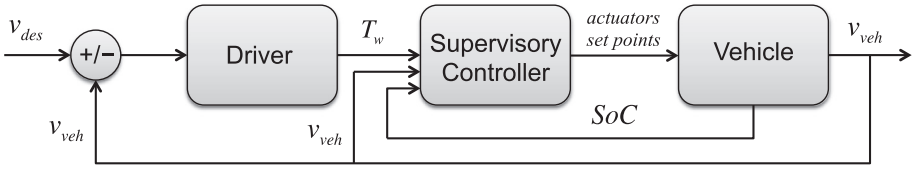

Fig. 2. Structure of the forward vehicle simulator for model-in-the-loop development.

is used. The level of detail of the vehicle component models and its forward-looking approach ensures reliable estimation of the fuel consumption. The simulator consists of longitudinal vehicle dynamics, battery state of charge (SoC) dynamics, stationary maps for MOT, GEN and ICE, a transmission model [23] and a supervisory controller for the in-vehicle energy management. In this paper, an experimentally validated battery pack model is used for model-in-the-loop design and simulation, that replaces the battery model provided with the original vehicle simulator. The replaced battery model is based on experimental data, from the LG Chem battery used in the Chevrolet Volt vehicle, collected at the Center for Automotive Research, The Ohio State University, and presented in the next Section 2.2. The simulator, whose modular structure is depicted in Fig. 2, consists of: *Driver* module, *Supervisory Controller* module, *Vehicle* module.

The *Driver* module contains information about the driving cycle, namely velocity and road grade, and implements a driver model (PID controller) to track the desired velocity profile, v_{des} in Fig. 2. It generates the torque requested at the wheels, T_w, needed to follow the desired speed profile, which is passed onto the *Supervisory Controller* module. The development and implementation of the energy management strategy to be used in the *Supervisory Controller* module of the vehicle simulator is the main focus of this paper and it is discussed in more details in the following sections. This module generates the setpoints of the actuators which are sent to *Vehicle* module. Those are: the torques of the engine and the electric motor, the speed of the generator, as well as the status of the three clutches. The setpoint values are applied to the three machines (MOT, GEN, ICE) and the status of the clutches defines the mode of operation of the powertrain. This can be one of the following: One-motor EV, Two-motor EV, Range-extender mode and Power-split mode, as discussed in Section 4. In addition, in the *Vehicle* module, the actual vehicle speed, v_{veh}, is obtained by integration of the vehicle dynamics equations, and fed back to the *Driver* and *Supervisory Controller* modules, together with the battery SoC.

2.1. Electric machines and internal combustion engine

The electric motor and the generator are modeled by means of their efficiency maps, shown in Figs. 3 and 4 while the engine is modeled with the brake specific fuel consumption (BSFC) map, from which the efficiency map is evaluated, as shown in Fig. 5.

2.2. Battery

The battery pack used in the GM Chevrolet Volt is composed of 288 LG Chem R1S3 Pouch Li-Ion cells, in a 96S 3P pack configuration, Parrish et al. [24]. Each cell has a nominal capacity, Q_{nom}, of 15 Ah and nominal voltage, V_{oc}, of 3.85 V [35].

A set of experimental tests were conducted to characterize the battery cell over different temperatures (−10 °C, 5 °C, 15 °C, 30 °C, 50 °C) and the entire domain of SoC range (0–100%). Fig. 6 shows the open-circuit voltage curves for different temperatures, and Fig. 7 show the battery internal resistance, R_0, (a) and battery capacity over the temperature envelope of [−10 °C ÷ 50 °C], (b).

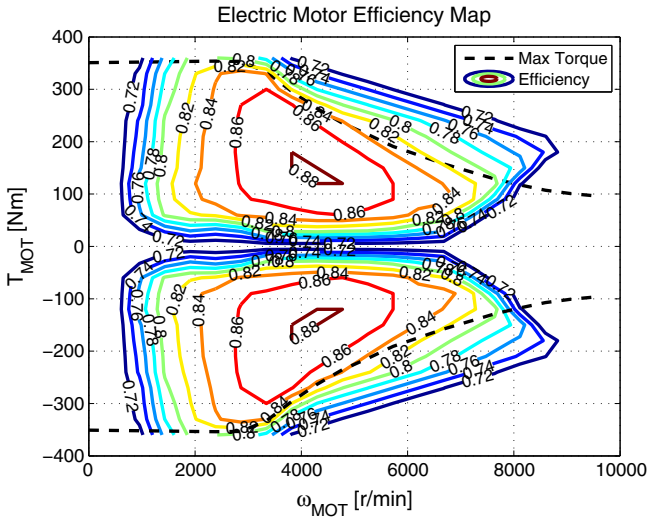

Fig. 3. Electric motor efficiency map [20,21].

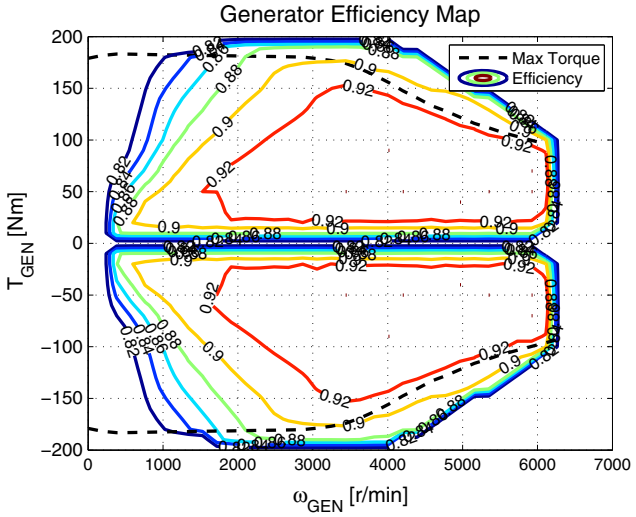

Fig. 4. Generator efficiency map [20,21].

The zero-*th* order equivalent circuit of Fig. 8 is used to model the battery in the vehicle simulator. This model has been demonstrated to be adequate to predict losses, in face of fast computational features, which are strictly needed when an energy-based simulator is used for control design purposes [3,26].

The battery load voltage, V_L, is obtained as:

$$V_L = V_{oc}(\text{SoC}) - I \cdot R_0(\text{SoC}) \tag{1}$$

where I is the current flowing in and out of the battery terminals (positive during discharge). In this study, the dependence of model parameters with the temperature has been neglected. In the case of

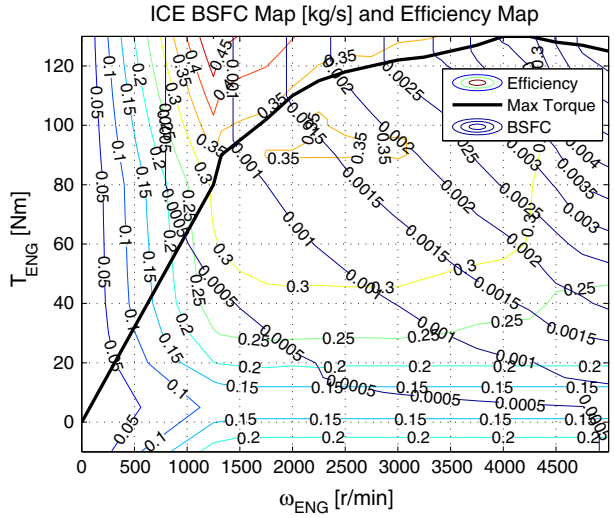

Fig. 5. Engine BSFC and efficiency map [21].

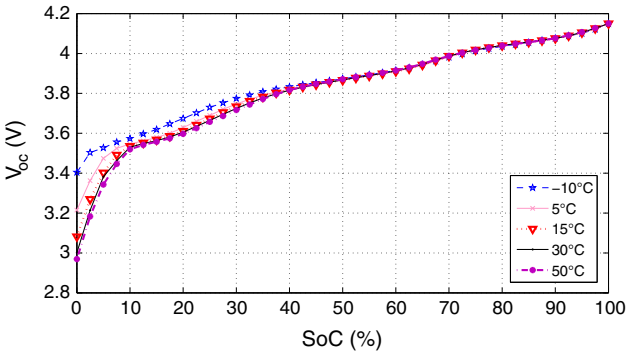

Fig. 6. Experimentally validated open-circuit voltage curves as a function of SoC for different temperatures.

the open-circuit voltage, this assumption is legitimated by experimental results, (Fig. 6 and [27]). In the case of the resistance, we leave the investigation of the dependence with respect to the temperature to future studies. On the other hand, the variation of battery open circuit voltage and internal resistance with respect to the SoC is not negligible, as shown in Fig. 6 and 9, and is accounted for in this study.

2.3. Planetary gear set

The transmission system of the Chevrolet Volt consists of a planetary gear set, shown in Fig. 1. The electric motor is connected to the sun, the generator is connected to the ring and the transmission output to the satellite carrier [21]. The kinematic Willis relation, Willis [28], links the speeds of ring (ω_r), sun (ω_s) and carrier (ω_c) as follows:

$$\rho \cdot \omega_r + \omega_s = \omega_c \cdot (\rho + 1) \tag{2}$$

where the constant parameter $\rho = 2.24$ represents the ratio between the number of teeth of the ring (N_r) and the teeth of the sun (N_s). As far as the torques at the gear set are concerned, the following relationship holds true:

$$\frac{T_r}{\rho} = \frac{T_c}{\rho + 1} = T_s \tag{3}$$

with T_r, T_s and T_c being the torques of ring, sun and carrier, respectively, for which the following relations hold:

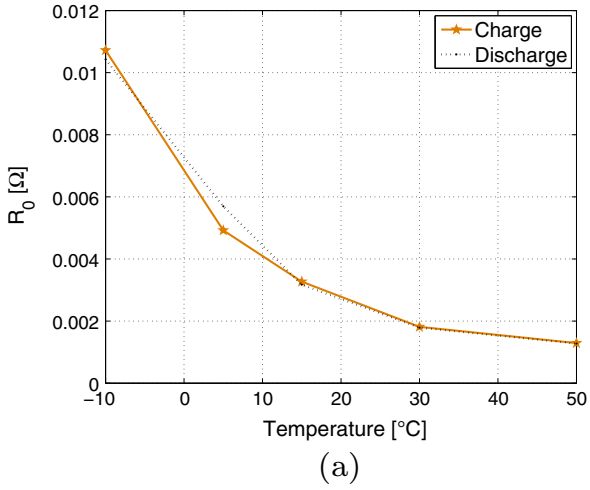

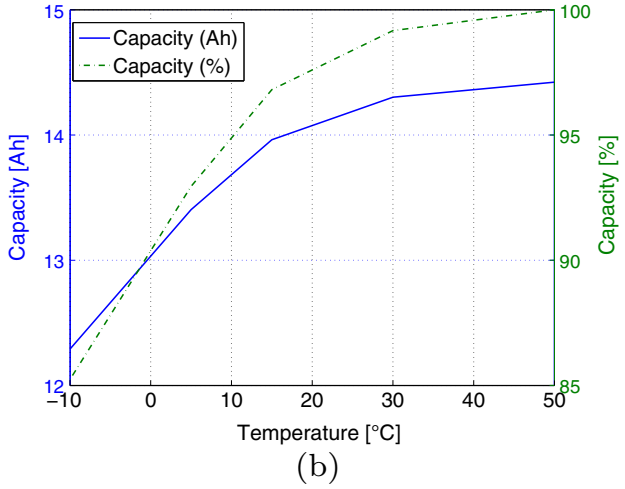

Fig. 7. Internal charge and discharge resistance (a) and capacity (b) as a function of temperature.

$$\begin{aligned} T_s &= T_{MOT} \\ T_r &= T_{GEN} + C3 \cdot T_{ICE} \\ T_c &= \frac{T_w}{f_d} \end{aligned} \tag{4}$$

where T_{MOT} and T_{GEN} are the motor and generator torques, respectively, while f_d, is the fixed gear ratio (final drive ratio) of the differential, which connects the output axle to the wheels.

2.4. Vehicle dynamics

The total force generated by the powertrain in the *Vehicle* module, F_{pwt}, is applied to the vehicle and the actual speed is then computed by integrating the longitudinal vehicle dynamics equation:

$$1.1 \cdot m \frac{d}{dt} v_{veh} = F_{pwt} + F_{tot} \tag{5}$$

where m is the vehicle mass, incremented by 10% to account for the rotational inertia of the components, while F_{tot} represents the total road load, which accounts for the aerodynamics and rolling resistance forces and the grade force for non-flat roads. The computed actual vehicle velocity, v_{veh}, is then fed back to the *Driver* module where it is compared to the desired vehicle velocity.

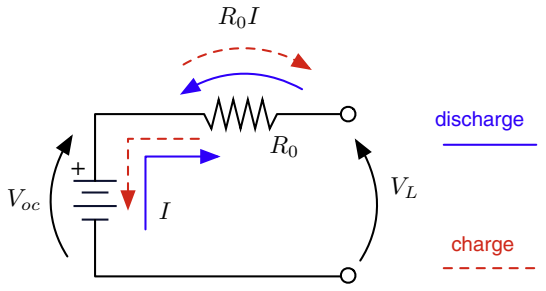

Fig. 8. Zero-*th* order electrical circuit model of the battery.

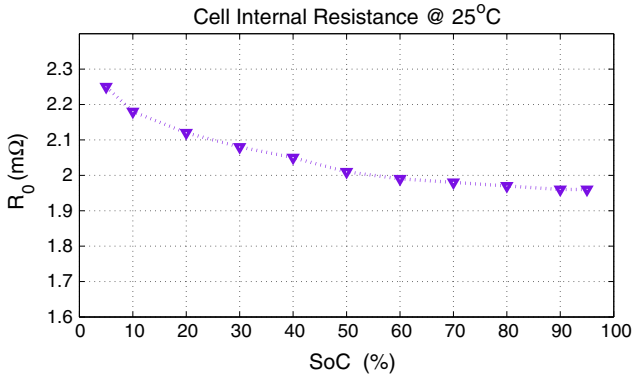

Fig. 9. Experimental data for battery cell internal resistance as a function of the SoC at 25 °C.

3. Optimal control problem formulation

The energy management problem for the Chevrolet Volt is cast into a constrained optimization problem aimed at minimizing the fuel consumed by the vehicle over a given trip while fulfilling the torque demanded by the driver and meeting the physical constraints of the powertrain components. Formally, the problem consists of minimizing the total mass of fuel, during a driving mission, or equivalently, minimizing the following cost function, $\mathcal{J}$:

$$\mathcal{J} = \int_{t_0}^{t_f} \dot{m}_f(u(t))\,dt \tag{6}$$

where $u(t)$ is the control action, $\dot{m}_f(u(t))$ is the instantaneous fuel consumption rate and $[t_0, t_f]$ is the optimization horizon. Typically, the choice is made such that $u(t) = P_{batt}(t)$ is the control input, Kim et al. [3], where P_{batt} is the battery power. Considering a quasi-static engine model, the fuel consumption is only a function of the engine torque and speed. As it will be discussed later, these variables can be related to the control input, P_{batt}, and the driver's power demand, P_w, that allows to express the fuel consumption as $\dot{m}_f(P_{batt}, P_w)$. The energy management problem, by its very nature, is a constrained optimization problem, where the objective function $\mathcal{J}$ is minimized under system dynamics constraints, instantaneous (local) constraints on the state and control, and finally integral (global) constraints on the state, as outlined in the following.

System dynamics: The battery SoC is the scalar state variable for the energy management problem and is predicted using the zero-th order model discussed in Section 2.2. The choice of SoC as the only state variable is due to the fact that the other components dynamics are much faster and it has been demonstrated in [4] that for the purpose of fuel economy estimation, they can be neglected.

Multiplying Eq. (1) by the current I on both sides, the battery power, P_{batt}, is expressed as:

$$P_{batt} = V_L \cdot I = V_{oc}(\mathrm{SoC}) \cdot I - I^2 \cdot R_0(\mathrm{SoC}) \tag{7}$$

Solving the algebraic equation – (7) – for the current, we obtain:

$$I = \frac{V_{oc}(\mathrm{SoC}) - \sqrt{V_{oc}(\mathrm{SoC})^2 - 4 \cdot P_{batt} R_0(\mathrm{SoC})}}{2R_0(\mathrm{SoC})} \tag{8}$$

The variation of the battery SoC is defined by the following equation:

$$\dot{\mathrm{SoC}} = -\eta_c \cdot \frac{I}{Q_{nom}} \tag{9}$$

where η_c represents the coulombic efficiency of the battery, Sciarretta and Guzzella [26] and Q_{nom} is the battery nominal capacity, as already mentioned. Therefore, the system dynamics, namely the SoC variation, can be expressed as a function of the battery power by replacing (8) into (9):

$$\begin{aligned}\dot{\mathrm{SoC}} &= -\eta_c \frac{V_{oc}(\mathrm{SoC}) - \sqrt{V_{oc}(\mathrm{SoC})^2 - 4 \cdot P_{batt} \cdot R_0(\mathrm{SoC})}}{2R_0(\mathrm{SoC})Q_{nom}} \\ &= f(\mathrm{SoC}(t), P_{batt}(t))\end{aligned} \tag{10}$$

The battery power in Eq. (10) can be calculated from the powertrain as a combination of the motor power, P_{MOT}, and the generator power, P_{GEN}, as follows:

$$\begin{aligned}P_{batt} &= \eta_{MOT}^{\gamma} \cdot P_{MOT} + \eta_{GEN}^{\gamma} \cdot P_{GEN} + P_{AUX} \\ &= \eta_{MOT}^{\gamma} \cdot T_{MOT} \cdot \omega_{MOT} + \eta_{GEN}^{\gamma} \cdot T_{GEN} \cdot \omega_{GEN} + P_{AUX}\end{aligned} \tag{11}$$

with P_{AUX} representing the auxiliary loads, η_{MOT} and η_{GEN}, the motor and generator efficiencies obtained from their corresponding efficiency maps, and $\gamma = 1$ in recuperating and $\gamma = -1$ in motoring.

Integral constraints: The integral constraints concern with initial and final values of SoC, namely $\mathrm{SoC}(t_0)$ and $\mathrm{SoC}(t_f)$, during PHEV operation over a given driving profile. These values are:

$$\mathrm{SoC}(t_0) = 0.95; \quad \mathrm{SoC}(t_f) = 0.3$$

and they indicate that a fully charged battery is available at the beginning of the trip and a 30% SoC threshold is selected to limit the activity of the battery at low state of charge.

Instantaneous constraints: Similarly to the integral constraints on battery SoC, there are instantaneous constraints imposed on the state and control variables that need to be satisfied at each instant of time. These constraints mostly concern with physical limits, such as the minimum and maximum torque and speed of ICE, MOT and GEN, and the minimum and maximum battery power and SoC:

$$\begin{aligned}&\mathrm{SoC}_{min} \leqslant \mathrm{SoC}(t) \leqslant \mathrm{SoC}_{max} \\ &P_{batt_{min}} \leqslant P_{batt}(t) \leqslant P_{batt_{max}} \\ &T_{x_{min}} \leqslant T_x(t) \leqslant T_{x_{max}} \\ &\omega_{x,min} \leqslant \omega_x(t) \leqslant \omega_{x,max}, \quad x = ICE, MOT, GEN\end{aligned} \tag{12}$$

where the subscript *min* represents the minimum threshold, while the subscript *max* represents the maximum threshold for the variables.

4. Pontryagin's Minimum Principle

In order to develop an on-line adaptive implementable strategy we first solve the optimal energy management problem applying the PMP [19,29], which provides a set of necessary conditions for the global optimality of a constrained optimization problem. As conditions on battery efficiency apply, according to [30], the necessary conditions of optimality provided by PMP are also sufficient, hence, they can be used to find the global optimal solution to the

energy management problem of PHEVs, provided that the driving cycle is known *a priori*.

In the PMP problem formulation the Hamiltonian function, H, is defined as:

$$H(\mathrm{SoC}(t), u(t), \lambda(t)) = \dot{m}_f(u(t)) + \lambda(t) \cdot \dot{\mathrm{SoC}}(t) \tag{13}$$

where $\lambda(t)$ is the co-state associated to the optimization problem and $\dot{\mathrm{SoC}}(t)$ is given by Eq. (10), Serrao et al. [31]. The PMP allows reducing the global optimization problem, described in the previous section, to a local instantaneous problem, consisting in finding the optimal control sequence $u^*(t)$ that minimizes the Hamiltonian function at each instant of time:

$$u^*(t) = \arg\min_{\boldsymbol{u}} H(\mathrm{SoC}(t), u(t), \lambda(t)) \tag{14}$$

while the state and the co-state evolve according to:

$$\dot{\mathrm{SoC}}(t) = \frac{\partial H}{\partial \lambda} = f(\mathrm{SoC}(t), P_{batt}(t)) \tag{15}$$

$$\dot{\lambda}(t) = -\frac{\partial H}{\partial \mathrm{SoC}} = -\lambda \frac{\partial \dot{\mathrm{SoC}}}{\partial \mathrm{SoC}} \tag{16}$$

In Eq. (16), the derivative of $\dot{m}_f$ as a function of the state variable SoC has been neglected since $\dot{m}_f$ is not an explicit function of SoC. Eqs. (15) and (16) represent a system of two first order differential equations in the variables $\mathrm{SoC}(t)$ and $\lambda(t)$, for which two boundary conditions are required, which are the initial and the final values of the SoC state, namely $\mathrm{SoC}(t_0)$ and $\mathrm{SoC}(t_f)$. Despite being completely defined, this two-point boundary value problem can be solved only numerically, by using the well-known *shooting method* [31].

While minimizing H, constraints are also enforced at each instant to ensure that the total power demand at the wheels is satisfied. Since in traction the vehicle can operate in four different modes – depending on the status of the clutches, $C1, C2$, and $C3$ – the power matching demand constraints are singled out below for each mode [23]:

1. *One-motor EV* ($C1 = 1, C2 = 0, C3 = 0$)[3]: only the electric motor propels the wheels, while the engine and generator set (GENSET) is switched off. The power requested at the wheels is:
$$P_w = P_{MOT} \tag{17}$$
Hence, in this mode there are not degrees of freedom as the power at the battery, from Eqs. (11) and (17), depends only on the driver's power demand, namely $P_{batt} = P_{batt}(P_w)$.
2. *Two-motor EV* ($C1 = 0, C2 = 1, C3 = 0$): the generator is connected to the planetary gear set but disconnected to the ICE. Hence, the driver's power demand is satisfied by both the electric motor and the generator, as given by:
$$P_w = P_{MOT} + P_{GEN} \tag{18}$$
By using the set of equations in Section 2.3, the torques from the devices are dictated from the torque at the wheels, while the speed of the generator, from Eq. (2), is the degree of freedom which can be optimally selected by the energy management strategy. From Eq. (11), P_{batt} is a unique function of the generator speed ω_{GEN}, for any given power demand P_w, *i.e.* $P_{batt}(\omega_{GEN}, P_w)$.
3. *Range-extender mode* ($C1 = 1, C2 = 0, C3 = 1$): this is a typical series mode of operation, with the electric motor alone driving the wheels, and the GENSET supplying power to the battery or directly to the electric motor. The power demanded at the wheels is satisfied by:
$$P_w = P_{MOT} \tag{19}$$
Under the range-extender mode kinematic constraints, Grebe and Nitz [21], it is possible to express $[T_{MOT}\ T_{GEN}]$ and $[\omega_{MOT}\ \omega_{GEN}]$ as a function of $[T_w\ \ T_{ICE}]$ and $[\omega_w\ \ \omega_{ICE}]$, making P_{batt} a function of T_{ICE} and ω_{ICE}, for any given power demand P_w, namely, $P_{batt} = P_{batt}(T_{ICE}, \omega_{ICE}, P_w)$. The variables, T_{ICE} and ω_{ICE} are selected to minimize the fuel consumption on each feasible engine operating line for a given P_w, making the GENSET operate along its *maximum efficiency line*[4] [31]. Thus, the dimension of the control problem reduces from two control variables, T_{ICE} and ω_{ICE} to only one, $P_{batt}(\omega_{GEN}, P_w)$, since also the fuel consumption $\dot{m}_f$ can be expressed as a function of P_{batt} only, *i.e.* $\dot{m}_f(P_{batt})$.
4. *Power-split mode* ($C1 = 0, C2 = 1, C3 = 1$): the three actuators - *i.e.*, electric motor, generator, engine - are all connected together through the planetary gear set with a variable speed ratio that depends on the generator speed, giving:
$$P_w = P_{MOT} + P_{GEN} + P_{ICE} \tag{20}$$
This mode allows transmitting mechanical power directly from the engine to the wheels. Under the power-split mode kinematic constraints, Grebe and Nitz [21], it is possible to express $[T_{MOT}\ T_{GEN}]$ and $[\omega_{MOT}\ \omega_{GEN}]$ as a function of $[T_w\ \ T_{ICE}]$ and $[\omega_w\ \ \omega_{ICE}]$ and, considering Eq. (20), it is immediate to see that P_{batt} can be expressed as a function of the unknown $[T_{ICE}\ \ \omega_{ICE}]$, for any given P_w, namely, $P_{batt} = P_{batt}(T_{ICE}, \omega_{ICE}, P_w)$. Following the same reasoning used for the *Range-extender* mode, in the *Power-split* mode operation, $P_{batt}(\omega_{GEN}, P_w)$ is still the only control variable used to minimize the fuel consumed while satisfying the power requested by the driver.

4.1. PMP implementation

When implementing the PMP on a vehicle simulator a few considerations need to be underlined, as far as the co-state dynamics and state boundary constraints are concerned.

4.1.1. Co-state λ

It is worth noting that the co-state variation with respect to time, Eq. (16), is different from zero if the system dynamic equation $f(\mathrm{SoC}(t), P_{batt}(t))$ is a function of the SoC and this is true given that the open-circuit voltage and the internal resistance of the battery depend on the SoC. Nonetheless, simulating the PMP, solving Eq. (15) and (16) with the *shooting method*, shows that the variation of $\lambda(t)$ with respect to time is negligible, as also found in [30–32], due to the fact that the battery efficiency is almost constant in this application. Fig. 10 shows that the co-state variation for a concatenation of NEDC cycles is within 0.005% overall variation from the initial value. As practically no variation of the co-state is taking place over vehicle operation, one can consider $\lambda(t) = \lambda_0\ \forall t \in [t_0, t_f]$ and determining λ_0, that solves the optimization problem, will guarantee optimality.

Moreover, from simulations studies, Sharma et al. [32], it has been shown that the optimal value of λ_0 is strongly dependent on the driving cycles and, for same velocity traces, it increases with the trip length. In [33], the authors have also analyzed the behavior of the optimal SoC trajectory under different road grade profiles; the optimal values of λ_0 and fuel consumptions have been compared for the same velocity traces and different grade profiles, confirming that for high-power demanding driving missions higher values of λ are required to maintain the SoC within the limits.

[3] A value of 1 means that the clutch is closed, while a value of 0 means that the clutch is opened.

[4] Practically speaking, the main limitation of this approach is in that the optimal operating points of the engine are calculated neglecting transient phenomena. This is a strong assumption but is justified by the fact that a quasi-static modeling approach is used.

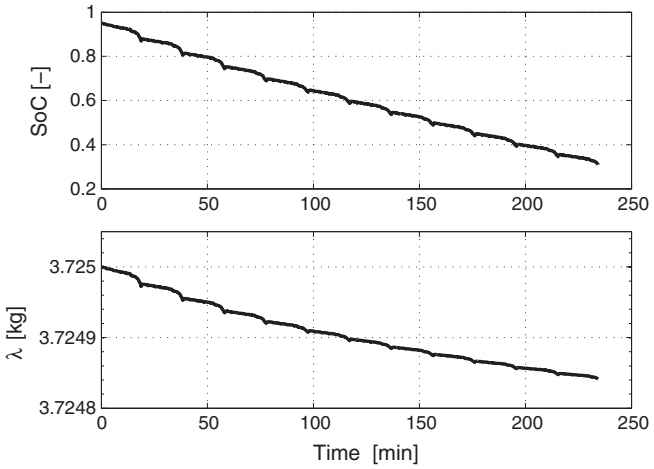

Fig. 10. Optimal SoC and λ profile with respect to time, obtained from PMP solution over a concatenation of 12 NEDC with no road grade variation.

Ultimately, the selection of the optimal (and unique) value of λ_0 varies from cycle to cycle, which is unknown, hence the on-line implementation of PMP cannot guarantee optimality. Nonetheless, the knowledge from PMP is used, in this study, to design a co-state adaptation algorithm that would make the energy management strategy based on PMP implementable in-real time, as highlighted in Section 5.

4.1.2. Penalty function

It is known that to ensure the global constraints on SoC to be met, a penalty function needs to be used in the Hamiltonian [4,19]. In the present study, an additive penalty function $\mu(\text{SoC})$ is considered, leading to:

$$H(\text{SoC},P_{batt},\lambda) = \dot{m}_f(P_{batt}) + [\lambda + \mu(\text{SoC},t)]f(\text{SoC},P_{batt}) \tag{21}$$

where, the penalty function is in the form of a piecewise SoC-dependent function given by:

$$\mu(\text{SoC}) = \begin{cases} K & \text{if SoC} < \text{SoC}_{min} = 0.30 \\ -K & \text{if SoC} > \text{SoC}_{max} = 0.95 \\ 0 & \text{else} \end{cases}$$

where K is a design parameter selected in simulations to ensure the SoC trajectory within the global constraints[5].

Within the operational range of the SoC (95% to 30%), the value of $\mu(\text{SoC})$ is zero and does not change the original formulation (see Eq. (13)). As soon as the SoC tends to go below the admissible limits, the penalty function (positive K) adds a cost to the battery usage that prohibits the optimizer to use the battery. Similarly, if the SoC tends to go above the upper limit of 0.95, the penalty function (negative K) decreases the cost of the battery inducing the optimizer to use the electric energy over the chemical energy.

5. Adaptive-PMP supervisory control strategy

In this section, we propose an algorithm to update the co-state λ as a result of changes in driving conditions. Inspired by the adaptation law proposed in [17] for charge sustaining HEVs, we design an adaptive energy management strategy based on PMP, hereafter A-PMP, able to guarantee suboptimal performances in PHEV operations. We make the assumptions that the average cycle speed (related to the mission typology) and the total traveled distance (this information may come from the GPS) are known and no information about the road grade is assumed.

The bottom plot of Fig. 11 shows the optimal SoC trajectory obtained after solving the PMP for the driving cycle of total length of 150 km, shown on the upper plot of Fig. 11 when no grade variation is considered (hereafter, No Grade scenario). The optimal SoC trend turns out to be a quasi-linear decreasing function of the total traveled distance, which is referred in literature to as blended strategy [11,15,32]. Fig. 12 portrays the optimal SoC trajectory for the grade profile with initial downhill signature shown in the upper plot of the same figure (hereafter, Downhill scenario), while Fig. 13 portrays the optimal SoC trajectory for the grade profile with initial uphill signature, shown in the upper plot of the same figure (hereafter, Uphill scenario). It can be seen that, when the road grade is different from zero, the global optimal solution from PMP does not exhibit a linear SoC trend, rather a zig-zag type of trend (along the grade profile) is followed. Thus, if the knowledge of upcoming grade were available or could be estimated, one could in principle think of feeding this information back to the energy management controller to better track the optimal non-linear SoC profile.

From these observations, we design an adaptation law that is composed of two parts: *tracking* and *reset*. The tracking phase consists in making the co-state (λ) change in order to ensure that the SoC is tracking a linear reference SoC profile, SoC_{ref}. In case of flat road this will guarantee tracking of optimal SoC profile. On the other hand, if the road is hilly, this will be far from being optimal, and to recover from an "unstable" SoC behavior a reset of the co-state to its initial value is implemented that brings the SoC profile to its initial trajectory trend.

5.1. Tracking

To guarantee a linear SoC profile tracking, the co-state λ_0 is updated based on the traveled distance, according to an auto-regressive moving-average (ARMA) filter:

$$\lambda(s+k) = \frac{\lambda(s)+\lambda(s-k)}{2} + K_p(\text{SoC}_{ref}(s) - \text{SoC}(s))) \tag{22}$$

In Eq. (22), k is the sampling distance, s is the current covered distance, and K_p is a proportional gain which corrects for divergences of SoC from the SoC_{ref}. The SoC_{ref} is an affine function of the current driven distance, s, that guarantees complete battery discharge, *i.e.* $\Delta\text{SoC} = 0.95 - 0.3$ over the total length of the trip, D_{tot}, assumed known.

A calibration study and a sensitivity analysis to optimally tune the adaptation law have been properly carried out in a previous work, Lacandia et al. [35], where the sampling distance and the proportional gain have been shown to have small influence on the fuel consumption, and a constant value can be selected, irrespective to the driving conditions. On the other hand, the parameter that results having the highest impact on optimality is the co-state, λ_0.

Fig. 14 shows a mapping between traveled distance and optimal λ_0 as a function of different driving cycles. The driving cycles used in this study have been classified in terms of average and maximum speeds, v_{avg} and v_{max}, as summarized in Table 2.

The results show that the optimal value of λ_0 is an initially monotonically increasing function of the traveled distance, reaching an asymptotic value as the distance increases beyond a certain value. This behavior is more pronounced for cycles with a higher average speed, while for cycles with a low average speed, *e.g.* NEDC, one can observe a slight increase of λ_0 with the distance.

These results can be implemented in the form of a look-up table where the optimal values of the co-state can be tabulated as a

[5] Different choices of penalty functions could have been done. In [34], it is proved that PMP using the penalty function $\mu(\text{SoC})$ (with $-K$ K bounds) is equivalent to the PMP formulation when using a term proportional to the violation in the penalty.

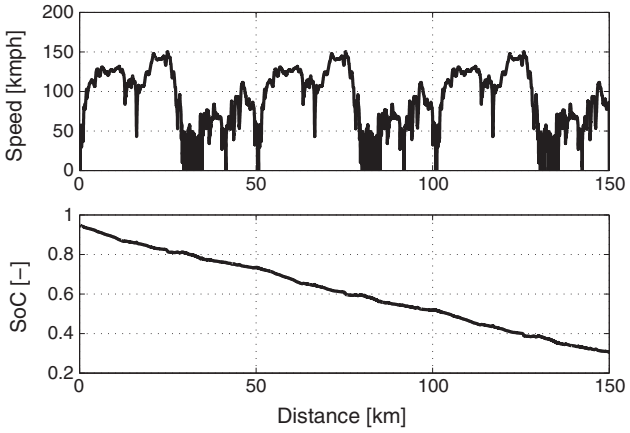

Fig. 11. Speed profile (with no grade) and optimal SoC profile.

function of total traveled distance and average driving cycle speed, thus generating the map shown in Fig. 15, which can be easily employed by the supervisory controller for co-state initialization purposes.

If the driving cycle (in terms of distance and average speed) is contained in the domain of the map of Fig. 15, then λ_0 can be directly obtained from it; otherwise λ_0 is set to be equal to one of the four boundary values of the map.

5.2. Reset

In the proposed adaptation law we assume that the desired SoC profile, SoC_{ref}, is linear with respect to the distance traveled. This is a reasonable approximation only if there is no road grade variation during the driving cycle.

In order to handle more realistic situations (*e.g.*, variation of grade), corrections to the adaptation law – Eq. (22) – are accounted for and implemented in the controller, which are only based on the knowledge of the distance to be traveled. These corrections are listed below:

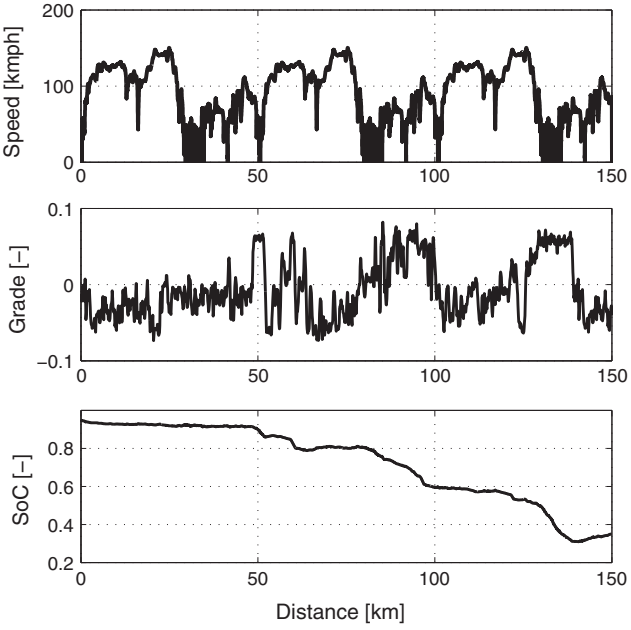

Fig. 12. Speed profile, grade profile (later referred to as Downhill) and optimal SoC trajectory.

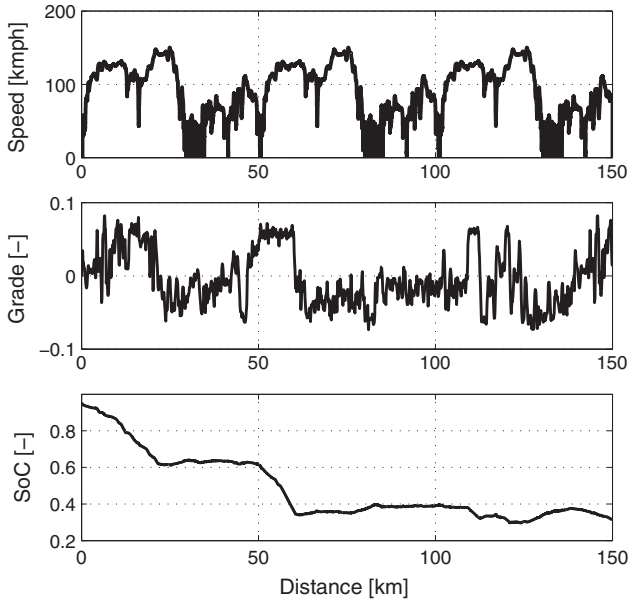

Fig. 13. Speed profile, grade profile (later referred to as Uphill) and optimal SoC trajectory.

1. In the presence of road grade, the SoC trend is not linear with respect to the distance (see Figs. 12 and 13), leading the actual SoC to cross the reference linear curve, thus making the condition $SoC(s) = SoC_{ref}(s)$ be verified. When this event occurs, the value of λ is reset and set equal to the initial value λ_0, avoiding instability of the SoC.
2. When the road grade variation is such that the battery is being charged at the very beginning of the trip ($s < 0.12D_{tot}$) or at the end of it ($s > 0.88D_{tot}$), the co-state is reset to zero. In fact, in a PHEV, the battery is expected to be completely charged at the beginning of the trip and it is reasonable to expect it to be discharged at the end. A value of λ equal to zero is imposed to virtually assign no costs to the use of the battery, to force using only the electric machines (enforcing the *All Electric* operating mode).
3. If $SoC(s) > 0.35$ when approaching the end of the trip ($s > 0.88D_{tot}$), $\lambda = 0$ is imposed, as in condition 2), to drive in *All Electric* mode and use the energy left in the battery to cover the remaining driving segment.

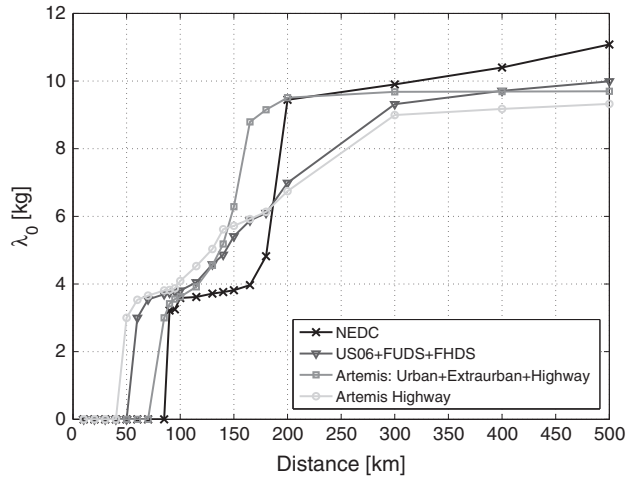

Fig. 14. Trend of λ_0 as a function of distance traveled for different driving cycles.

Table 2
Driving cycles features.

Cycle	v_{avg} (km/h)	v_{max}(km/h)
NEDC	33.6	120
US06+FUDS+FHDS	54.5	129
Artemis Urban+Extraurban+Highway	61.1	150
Artemis Highway	99.5	150

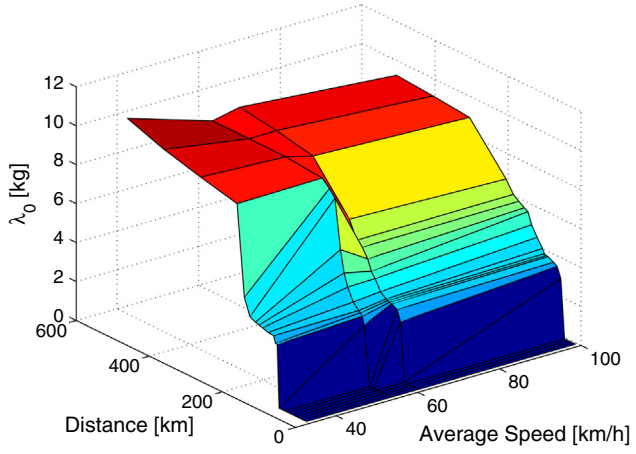

Fig. 15. Map with the values of λ_0 as a function of distance and average speed.

Fig. 16 shows the supervisory controller logic within the vehicle model. The required information on the total traveled distance and the average cycle speed are used to initialize the co-state λ_0, according to map in Fig. 15 thus enabling the execution of the A-PMP (Eq. (22)), from SOC feedback. A series of conditions is then verified to decide upon the mode of operation of the powertrain. To prevent the battery SoC to drop below the minimum allowable threshold (30% SoC), the supervisory controller select the series mode with the GENSET running at maximum power (referred to as "Max GENSET Power" in Fig. 16). This mode is activated by the supervisory controller every time a driving cycle with severe road grade combined with high speeds occurring at SoC $\sim$ 0.3 is detected. When the supervisory controller reads $\lambda = 0$, it then selects *All Electric* mode as mode of operation. Also, to avoid cranking dynamics, the speed of the GENSET, ω_{GENSET}, is kept at least equal to the idle speed of the thermal engine, $\omega_{ICE,idle}$, *i.e.* $\omega_{GENSET} = \omega_{GEN} = \omega_{ICE} \geqslant \omega_{ICE,idle}$.

6. Simulation results

In the following, results of the adaptive strategy, tested by using No Grade (Fig. 11), Downhill (Fig. 12) and Uphill (Fig. 13) scenarios, are presented. In particular, these scenarios present three different altitude profiles for the same speed trace, which is composed by a combination of three Artemis cycles, namely highway, urban and extraurban, for a total length of 150 km (see upper plot of Fig. 11). The proposed adaptive energy management algorithm is then compared to the optimal solution from PMP and the on-board implemented strategy, *i.e.* CD/CS.

In simulating the CD/CS strategy, the depletion of the battery is achieved by making the powertrain work in *One Motor EV* or *Two Motor EV* modes, depending on the power request, which is satisfied first by the motor and then, if needed, by the generator. The SoC is then sustained, in the charge sustaining segment, by means of an Adaptive-ECMS algorithm, Onori et al. [17], which ensures that the SoC is sustained at around 0.3 SoC.

Fig. 17 shows the A-PMP SoC profile, compared to the two other strategies along with the SoC linear reference curve, for the first scenario (No Grade). It can be seen how the A-PMP trajectory follows the reference SoC trend (black dashed line) resulting in a quasi-linear trajectory with the distance similar to the optimal PMP solution (gray dot-dashed curve). The behavior of the adapted co-state is also shown. It can be seen that the value of λ_0 is set to its initial value whenever the SoC crosses the SoC_{ref}.

Fig. 18 portrays the SoC trajectories for the Downhill scenario. In this case, the selection of a λ equal to zero is performed at the beginning and towards the end of the driving cycle to implement the rule 2.

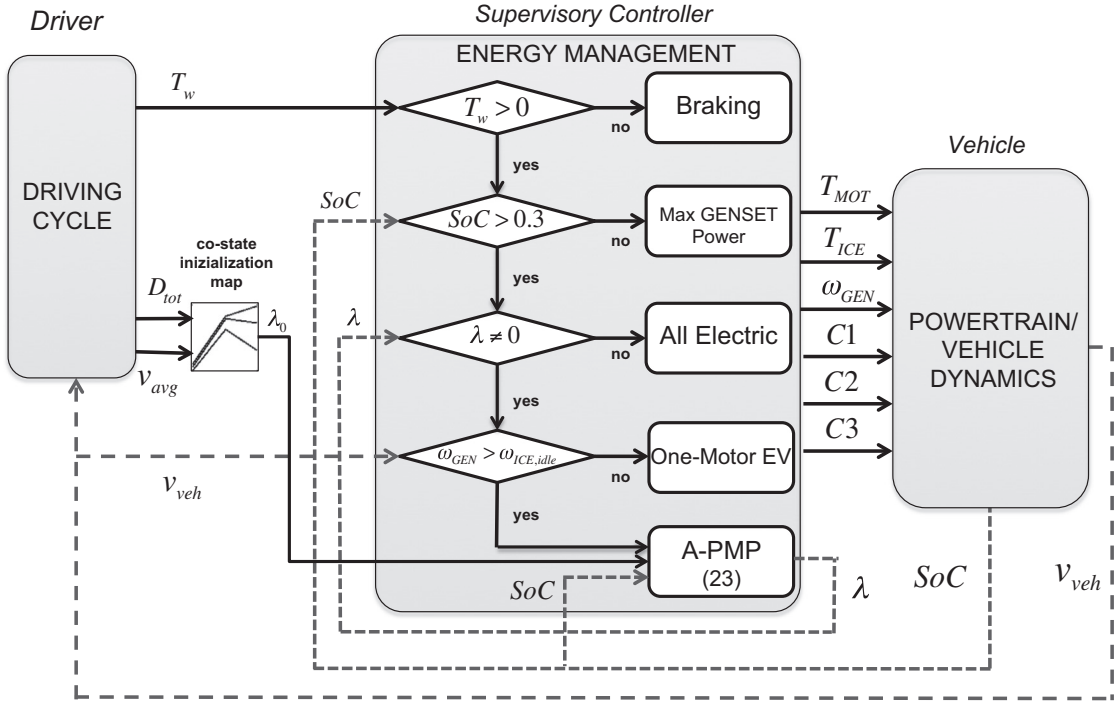

Fig. 16. Supervisory controller logic for powertrain mode selection.

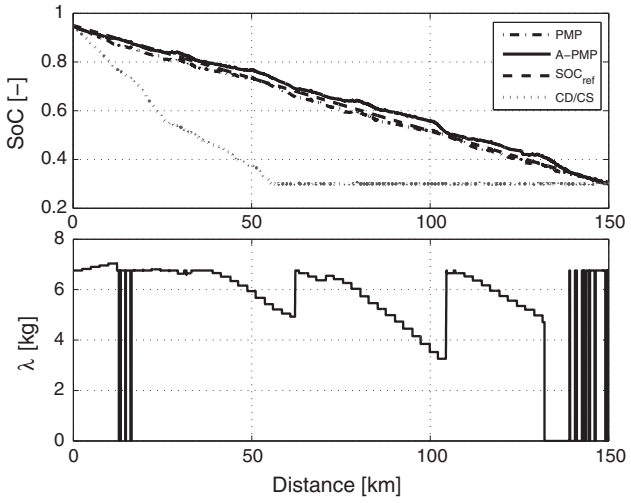

Fig. 17. SoC profiles (A-PMP, PMP, CD/CS and linear SoC reference) and λ trajectory versus the traveled distance (No Grade).

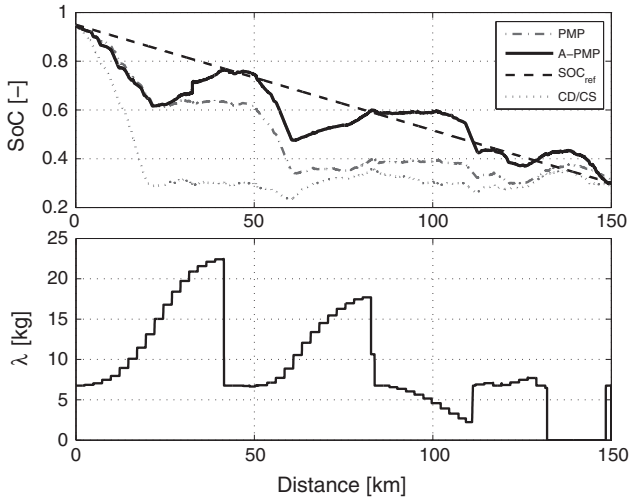

Fig. 19. SoC profiles (A-PMP, PMP, CD/CS and linear approximation) and λ trajectory versus the traveled distance (Uphill).

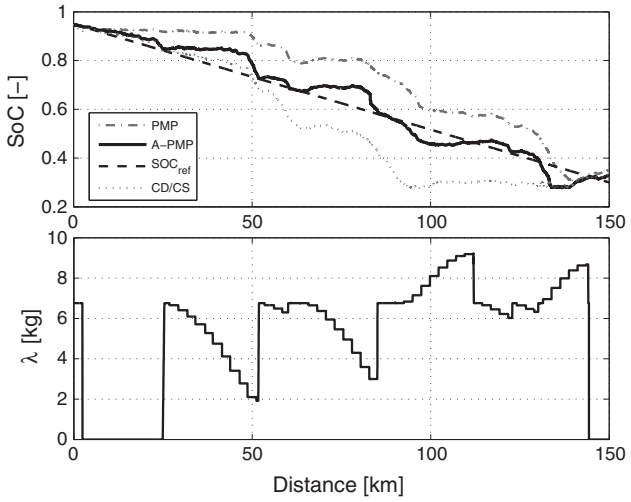

Fig. 18. SoC profiles (A-PMP, PMP, CD/CS and linear approximation) and λ trajectory versus the traveled distance (Downhill).

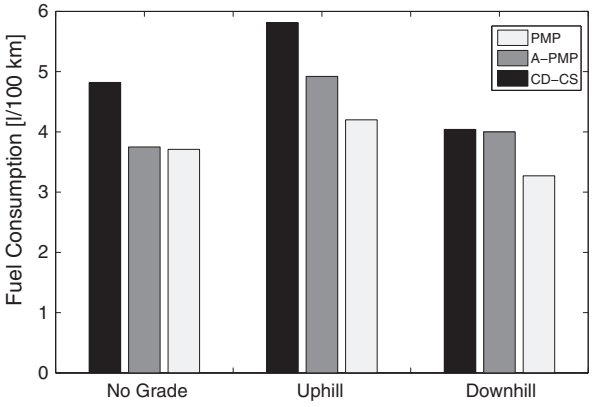

Fig. 20. Comparison of the fuel consumption obtained with the three strategies in the different scenarios.

Fig. 19 portrays the SoC trajectories for the Uphill scenario, showing that the optimal SoC trajectory (gray dot-dashed line) diverges significantly from the linear reference (black dashed line), unlike the A-PMP trajectory (black line). In particular, the optimal solution lets the battery be discharged as a consequence of the frequent uphills, while the A-PMP sometimes "forces" the battery to be charged, also during climbing paths, in order to follow the linear SoC reference. This is also reflected by the adapted co-state which is often greater than the optimal value (*i.e.* $\lambda_{opt} = 8.7$ kg for Uphill), as shown in bottom plot of Fig. 19, so discouraging the battery discharge. A similar behavior can be observed for the Downhill scenario, where the co-state is often lower than the optimal value (*i.e.* $\lambda_{opt} = 5.34$ kg for Downhill), as it can be seen in the bottom plot of Fig. 18. In fact, to follow a linear SoC reference, the A-PMP discharges the battery when possible to face the frequent charges due to the recurring downhills.

Fig. 20 and Table 3 give a comparison of fuel consumptions in liters per 100 km and in percentage, respectively, obtained from the A-PMP strategy compared to the optimal solution from the PMP and the CD/CS. In Table 3, percentages are provided both in terms of actual fuel consumption, $\frac{\Delta l/100\text{ km}}{(l/100\text{ km})_{PMP}}$ and $\frac{\Delta l/100\text{ km}}{(l/100\text{ km})_{CD/CS}}$, and of equivalent fuel consumption,[6] $\frac{\Delta l_e/100\text{ km}}{(l_e/100\text{ km})_{PMP}}$ and $\frac{\Delta l_e/100\text{ km}}{(l_e/100\text{ km})_{CD/CS}}$. As expected, the A-PMP performs better with no grade variations, since the reference SoC trajectory to be tracked is very close to the optimal PMP trajectory. In particular, the A-PMP goes from a maximum increase in consumption of 28.13% (with respect to the optimal solu-

Table 3
A-PMP fuel consumption comparison in percentage w.r.t. PMP and CD/CS.

	A-PMP vs PMP		A-PMP vs CD/CS	
	$\frac{\Delta l/100\text{ km}}{(l/100\text{ km})_{PMP}}$	$\frac{\Delta l_e/100\text{ km}}{(l_e/100\text{ km})_{PMP}}$	$\frac{\Delta l/100\text{ km}}{(l/100\text{ km})_{CD/CS}}$	$\frac{\Delta l_e/100\text{ km}}{(l_e/100\text{ km})_{CD/CS}}$
No grade	+1.08%	+0.47%	−22.20%	−14.13%
Uphill	+17.14%	+9.78%	−15.32%	−10.39%
Downhill	+28.13%	+15.14%	−0.99%	−1.04%

[6] The equivalent fuel mass, over a given driving event, in equivalent liters per 100 km, $l_e/100$ km, was calculated considering the energy the engine should provide to produce the net amount of energy supplied by the battery E_{batt}, corrected with the lower heating value (LHV) of the fuel and an average engine efficiency, $\overline{\eta}_{ICE}$, Paganelli et al. [2]:

$$m_{f,eq} = \frac{E_{batt}}{LHV \cdot \overline{\eta}_{ICE}} \tag{23}$$

tion), given by the Downhill scenario, to an increase of only 1.08%, if no road grade variations were considered. This trend is similar both in terms of actual fuel consumption and of equivalent fuel consumption. With regard to the CD/CS strategy, the adaptive strategy presented in this study reduces fuel use by around 22.2% (with no grade), which corresponds to a 14.13% reduction in equivalent fuel consumption. In Downhill, instead, only a 0.99% reduction in actual used fuel, corresponding to a 1.04% reduction in equivalent fuel consumption, is obtained. This is mainly due to the last segment of the SoC that flattens at 30%, where, to avoid drops of the SoC under this value, the GENSET works at maximum power.

7. Conclusions

In this paper we proposed an adaptive supervisory control strategy based on the Pontryagin's Minimum Principle for solving the on-line energy management problem in the GM Chevrolet Volt.

Despite the fact that the optimal solution of the energy management problem using PMP can be obtained only via off-line implementation, where an iterative search for λ is possible, the non-causal nature of the PMP strategy was used to design a causal controller, referred to as A-PMP, where the co-state is adapted as driving conditions change. The average vehicle speed and the total traveled distance are the only parameters assumed known (even if in practice they can be affected by measurement or prediction uncertainties). Nevertheless, the proposed adaptation law assures robustness against changing in driving conditions and also uncertainties in those parameters, due to its feedback mechanism. The proposed novel adaptation law operates over a distance based domain and is equipped with rules to prevent divergence of the actual SoC from a reference linear SoC profile, by means of a suitable reset of the co-state.

A comparative analysis of the A-PMP with the optimal PMP, and CD/CS was presented. Fuel consumption and SoC profiles were compared for the three strategies under different driving profiles, with a particular attention to the variation in the road topography.Results have shown that the new proposed design can achieve improvements in fuel consumption around 20%. It was found that the A-PMP well approximates the optimal PMP solution, under zero road grade scenario, unlike the CD/CS strategy, which must work in *Range-extender* mode, in order to sustain the battery charge, resulting in higher fuel consumption. At the same time, with road grade variations, relevant changes in the co-state value cannot be prevented in order to track the SoC linear reference, which does not represent the optimality anymore. This way, the controller can sometimes provide results quite far from the optimal ones, albeit still performing better than the in-vehicle CD-CS strategy. A thorough prediction of upcoming driving conditions may improve the performance of the A-PMP, as this information could be fed back to the controller to better track the optimal SoC profile. On the other hand, this was out of the scope of the present paper, where only average speed and traveled distance were used to feed the supervisory controller. Future studies could be addressed at improving this aspect.

References

[1] Markel T, Smith K, Pesaran A. PHEV energy storage performance/life/cost tradeoff analysis. In: 8th advanced automotive battery conference, Tampa, FL; 2008.

[2] Paganelli G, Ercole G, Brahma A, Guezennec Y, Rizzoni G. General supervisory control policy for energy optimization of charge-sustaining hybrid electric vehicles. JSAE Rev 2001;22(4):511–8.

[3] Kim N, Cha S, Peng H. Optimal control of hybrid electric vehicles based on Pontryagin's Minimum Principle. IEEE Trans Control Syst Technol 2011;19(5):1279–87.

[4] Sciarretta A, Guzzella L. Control of hybrid electric vehicles. Control Syst IEEE 2007;27(2):60–70.

[5] Hung Y-H, Wu C-H. An integrated optimization approach for a hybrid energy system in electric vehicles. Appl Energy 2012;98:479–90.

[6] Tribioli L, Fumarola A, Martini F. Methodology procedure for hybrid electric vehicles design. In: SAE technical papers; 2011. doi: http://dx.doi.org/10.4271/2011-24-0071.

[7] Wu X, Cao B, Li X, Xu J, Ren X. Component sizing optimization of plug-in hybrid electric vehicles. Appl Energy 2011;88(3):799–804.

[8] Hu X, Murgovski N, Johannesson L, Egardt B. Energy efficiency analysis of a series plug-in hybrid electric bus with different energy management strategies and battery sizes. Appl Energy 2013;111(0):1001–9.

[9] Lin C, Kang J, Grizzle J, Peng H. Energy management strategy for a parallel hybrid electric truck. In: Proceedings of the 2001 American control conference. vol. 4; 2001. p. 2878–83.

[10] Khayyam H, Bab-Hadiashar A. Adaptive intelligent energy management system of plug-in hybrid electric vehicle. Energy 2014;69(0):319–35.

[11] Tulpule P, Marano V, Rizzoni G. Energy management for plug-in hybrid electric vehicles using equivalent consumption minimisation strategy. Int J Electr Hybrid Veh 2010;2(4):329–50.

[12] Onori S, Spagnol P, Marano V, Guezennec Y, Rizzoni G. A new life estimation method for lithium-ion batteries in plug-in hybrid electric vehicle applications. Int J Power Electr 2012;4(3):302–19.

[13] Larsson V, Johannesson L, Egardt BS, Lasson A. Benefit of route recognition in energy management of plug-in hybrid electric vehicles. In: American control conference, Montreal, Canada; 2012.

[14] Zhang C, Vahidi A. Route preview in energy management of plug-in hybrid vehicles. IEEE Trans Control Syst Technol 2012;20(2):546–53.

[15] Yu H, Kuang M, McGee R. Trip-oriented energy management control strategy for plug-in hybrid electric vehicles. In: Proceedings of the IEEE conference on decision and control and european control conference; 2011. p. 5085–5812.

[16] Katranik T. Analytical method to evaluate fuel consumption of hybrid electric vehicles at balanced energy content of the electric storage devices. Appl Energy 2010;87(11):3330–9.

[17] Onori S, Serrao L, Rizzoni G. Adaptive equivalent consumption minimization strategy for HEVs. In: ASME dynamic systems and control conference; 2010.

[18] Ambuhl D, Guzzella L. Predictive reference signal generator for hybrid electric vehicles. IEEE Trans Veh Technol 2009;58(9):4730–40.

[19] Geering H. Optimal control with engineering applications. Springer; 2007.

[20] Miller MA, Holmes AG, Conlon BM, Savagian PJ. The GM Voltec 4ET50 multi-mode electric transaxle, SAE 2011-01-0887.

[21] Grebe UD, Nitz LT. VOLTEC – the propulsion system for Chevrolet Volt and Opel Ampera, MTZ Worldwide Edition, vol. 72, 05-2011.

[22] Sciarretta A, Serrao L, Dewangan P, Tona P, Bergshoeff E, Bordons C, et al. A control benchmark on the energy management of a plug-in hybrid electric vehicle. Control Eng Pract 2014;29:287–98.

[23] Falieres Q, Grasset O, Roblet K, Xu Y, Noiret C, Serrao L, Sciarretta A. A contradictory analysis of GM Voltec powertrain. In: European electric vehicle conference, 2011.

[24] Parrish R, Elankumaran K, Gandhi M, Nance B, et al., Voltec Battery Design and Manufacturing, SAE 2011-01-1360.

[25] Sciarretta A, Guzzella L. Vehicle propulsion systems: introduction to modeling and optimization. Springer; 2005.

[26] Plett GL. Sigma-point Kalman filtering for battery management systems of lipb-based hev battery packs Part 2: Simultaneous state and parameter estimation. J Power Sources 2006;161(2):1369–84.

[27] Willis R. Principles of mechanism. 2nd ed. Longmans, Green and Co.; 1870.

[28] Kirk DE. Optimal control theory, an introduction. Englewood Cliffs, NJ: Prentice-Hall; 1970.

[29] Kim N, Rousseau A. Sufficient conditions of optimal control based on Pontryagin's minimum principle for use in hybrid electric vehicles, IMechE Part D: J Automobile Eng 2012.

[30] Serrao L, Onori S, Rizzoni G. A comparative analysis of energy management strategies for hybrid electric vehicles. Dyn Syst Meas Control J 2011;133(3):031092 (p. 9).

[31] Sharma O, Onori S, Guezennec Y, Analysis of Pontryagins Minimum Principle-based energy management strategy for PHEV applications. In: 5th annual dynamic systems and control conference and 11th motion and vibration conference, Fort Lauderdale, FL; 2012.

[32] Tribioli L, Onori S, Analysis of energy management strategies in plug-in hybrid electric vehicles: application to the Chevrolet Volt. In: Proceedings of the American control conference; 2013.

[33] Serrao L, Onori S, Rizzoni G. ECMS as a realization of Pontryagin's Minimum Principle for HEV control. In: American control conference; 2009.

[34] Lacandia F, Tribioli L, Onori S, Rizzoni G. Adaptive Energy Management Strategy Calibration in PHEVs based on a Sensitivity Study, SAE 2013-24-0074.

[35] Cordoba-Arenas A, Onori S, Guezennec Y, Rizzoni G. Capacity and power fade cycle-life model for plug-in hybrid electric vehicle lithium-ion battery cells containing blended spinel and layered-oxide positive electrodes. J Power Sources 2015;278:473–83.